Hindawi
Geofluids
Volume 2021, Article ID 8827721, 17 pages
https://doi.org/10.1155/2021/8827721

Research Article

Microscopic Residual Oil Distribution Characteristics and Quantitative Characterization of Producing Degree Based on Core Fluorescence Analysis Technology

Huifen Xia,[1] Lihui Wang,[1] Peihui Han,[2] Ruibo Cao,[2] Siqi Zhang,[1] and Xianda Sun[1]

[1]*School of Petroleum Engineering, Northeast Petroleum University, Daqing Heilongjiang 163318, China*
[2]*Research Institute of Exploration and Development of Daqing Oilfield Company Ltd., Daqing Heilongjiang 163712, China*

Correspondence should be addressed to Lihui Wang; huiaixin120710@163.com

Received 18 July 2020; Revised 4 November 2020; Accepted 17 November 2020; Published 6 January 2021

Academic Editor: Guozhong Hu

In this study, to address the insufficiency of research on the distribution characteristics and quantitative characterization of oil, water, and rock in a reservoir, laser confocal and core fluorescence analysis techniques are combined with core flooding experiments to investigate oil–water distribution characteristics in the core and the microscopic origin of residual oil. The results obtained show that the three-dimensional (3D) distribution characteristics of oil, water, and rock can be depicted using a laser confocal technique. Free and bound states are dominated by water flooding, and their total proportion is 93.65%, while the semibound state only accounts for 6.35% of the total. Polymer flooding has clear effects such as production of cluster-like residual oil, interparticle adsorption state residual oil, pore surface oil film, and corner residual oil. After alkali-surfactant-polymer (ASP) flooding, the residual oil produced at the lowest degree corresponds to particle adsorption oil, pore surface oil films, and interparticle adsorption state residual oil. The emulsion transition process in porous media, i.e., Winsor I→Winsor III→Winsor II, is studied. Moreover, the fluorescence analysis technology is used to clarify the causes for residual oil production, namely, pore structure, crude oil viscosity, the Jia Min effect, particle migration, and adsorption capacity. The combination of laser confocal and fluorescence analysis technology can help realize the three-dimensional reconstruction of the fluid in the core, and it can quantitatively characterize the microscopic residual oil. According to the analysis results, it can also guide the formulation and adjustment of oilfield development plans.

1. Introduction

Reservoir residual oil saturation forms the basis for the formulation and adjustment of oilfield development plans and improvement of oil recovery [1, 2]. Most oilfields in China are experiencing high water cuts; further, because of the complex geological conditions of these oilfields and the large differences in the nature of crude oil, 70% of the residual oil remains underground. In this regard, two aspects that significantly aid oilfield development are (i) an accurate description of the oil–water distribution characteristics and the genesis of residual oil in the reservoir [3, 4] and (ii) a quantitative characterization of the residual oil content. Therefore, it is necessary to describe the macro- and microdistributions of residual oil accurately [5].

Currently, the research and development of residual oil has progressed from macrotechnical approaches to fine microrecognition ones to meet increasing requirements; further, certain results regarding microresidual oil analyses have been achieved. Chen et al. used a fluorescence microscope excited by ordinary blue light to calculate the microscopic oil saturation according to the color of different positions in the fluorescent slice image; they finally determined the exact ratios of rock, oil, and water in the fluorescent slice. When compared with traditional estimation methods, this method can analyze microscopic residual oil quickly and easily, and it can also eliminate human interference and achieve better accuracy [6]. Sun et al. employed micronano computed tomography to attenuate different degrees in the core via X-rays, and they reconstructed the three-dimensional morphology of the rock

skeleton pore structure using two-dimensional projection image acquisition and three-dimensional data without incurring damage or requiring high resolution [7]. Di et al. used low-field nuclear magnetic resonance to analyze the difference between the absorption and reflection of the pulse signal using pores and fluids that emit radio frequency pulses, and they inversely calculated the relaxation curve T2 spectrum; this spectrum showed the saturation of the movable fluid in the core and the characteristics of the pore structure, and the parameters were calculated [8]. Fan et al. used a visual model of glass etching and a simplified pore model to simulate the pore structure of the formation. According to the occurrence state and distribution characteristics of the microscopic residual oil in the model after different oil displacement systems being employed, a microscopic visualization oil displacement system can be used to calculate the residual oil saturation in the model [9].

However, the above research methods have the following disadvantages:

(1) The original state and positional relationship of crude oil and water cannot be guaranteed during sample preparation

(2) During image acquisition, a suitable optical path system is not selected; therefore, the fluorescence colors of oil and water are similar, and the oil–water interface cannot be distinguished clearly. Therefore, the interpretation of the bound state, semibound state, and free state appears to be insufficiently evidenced or has large errors

(3) There exists a lack of visualized microdistribution research on crude oil

(4) The three-dimensional analysis and detection of oil–water–rock cannot be performed via ordinary fluorescence microscopes. The CT images can neither clearly distinguish nor classify and quantitatively characterize the fluid in the pores. The low-field nuclear magnetic emission pulse signal has a limited penetration ability, which generates a feedback that is not sufficiently accurate; the detection needs to cut the core; and the required size is limited, because of which the true condition of the fluid in the core cannot be reflected

(5) Microscopic simulation model technology often differs significantly from the actual reservoir development, and this is difficult to explain reasonably.

In this study, laser confocal and cryopreservation fluorescence microscopy were used to investigate the microscopic residual oil quantitative distribution and occurrence mechanism characteristics and to analyze the oil–water distribution and emulsification phenomenon in the porous medium; the analysis process is shown in Figure 1. The technology and methods used in this study are original and advanced. Currently, few studies have investigated this field, especially in the context of tertiary oil recovery and the determination of microscopic residual oil saturation after ASP flooding and polymer flooding. The proposed method exhibits considerable potential for application in research on residual oil in other oil fields, and it presents a strong guiding significance and practicality [10–12].

2. Materials and Methods

2.1. Materials. According to the on-site test performed in the Daqing Oilfield, polyacrylamide with a molecular weight of 12 million and a concentration of 2200 mg/L was used in the polymer flooding experiment. The component concentration of the ternary composite system includes a polymer concentration of 2200 mg/L + 1.2%alkali + 0.3%surfactant; the surfactant is petroleum sulfonate, and the alkali is sodium carbonate. The component chemical parameters are listed in Table 1.

According to the on-site application at the Daqing Oilfield, all flooding systems use clean water to configure mother liquor, sewage diluting target fluid, and saturated water, and water flooding uses sewage. This is implemented to save clean water resources and effectively use the flowback sewage. According to the on-site water quality test results, the NaCl content of clean water is 950 mg/L, and that of sewage is 4500 mg/L. Therefore, an experiment involving simulated water with the same NaCl contents can recreate on-site injection conditions. The experimental oil involves a simulated oil prepared using crude oil and kerosene produced in the field in a certain ratio, with a viscosity of 10 mPa s to simulate the viscosity of crude oil under the formation conditions at the Daqing Oilfield; core parameters are shown in Table 2.

2.2. Methods. Figure 2 shows a schematic to illustrate the difference between conventional core flake preparation and frozen core preparation. According to the test results, the thickness of the sample is greater than 1 mm in the conventional slicing method, which causes fluorescence interference between the upper and lower pores; slicing at 20°C would destroy the initial state of the oil–water distribution and result in an inconspicuous distinction between oil, water, and minerals, thereby affecting the analysis results as shown in Figure 2(a). After the freeze filming process, the initial state of the oil–water distribution is maintained, and the thickness of the sheet is less than 0.05 mm; this avoids the upper and lower occlusion of particles and fluorescence interference, and it results in the oil–water interface being clearly distinguishable, as shown in Figure 2(b).

After the oil displacement experiment, the core was placed in liquid nitrogen for low-temperature storage to maintain the original oil–water distribution in the core. Because the simulated oil is prepared using crude oil and kerosene, kerosene volatilizes under normal temperature conditions and affects the oil saturation in the core. However, the low-temperature environment formed by the quick freezing of liquid nitrogen can prevent the volatilization of the fluid and form a shield on the surface of the core to prevent the fluid from reacting with air. After storage for 12 h, the fluid in the core stabilized, and the film was produced. Core slices 2 cm thick were cut at the injection, middle, and production ends, as shown in Figure 3(a). To avoid the heat

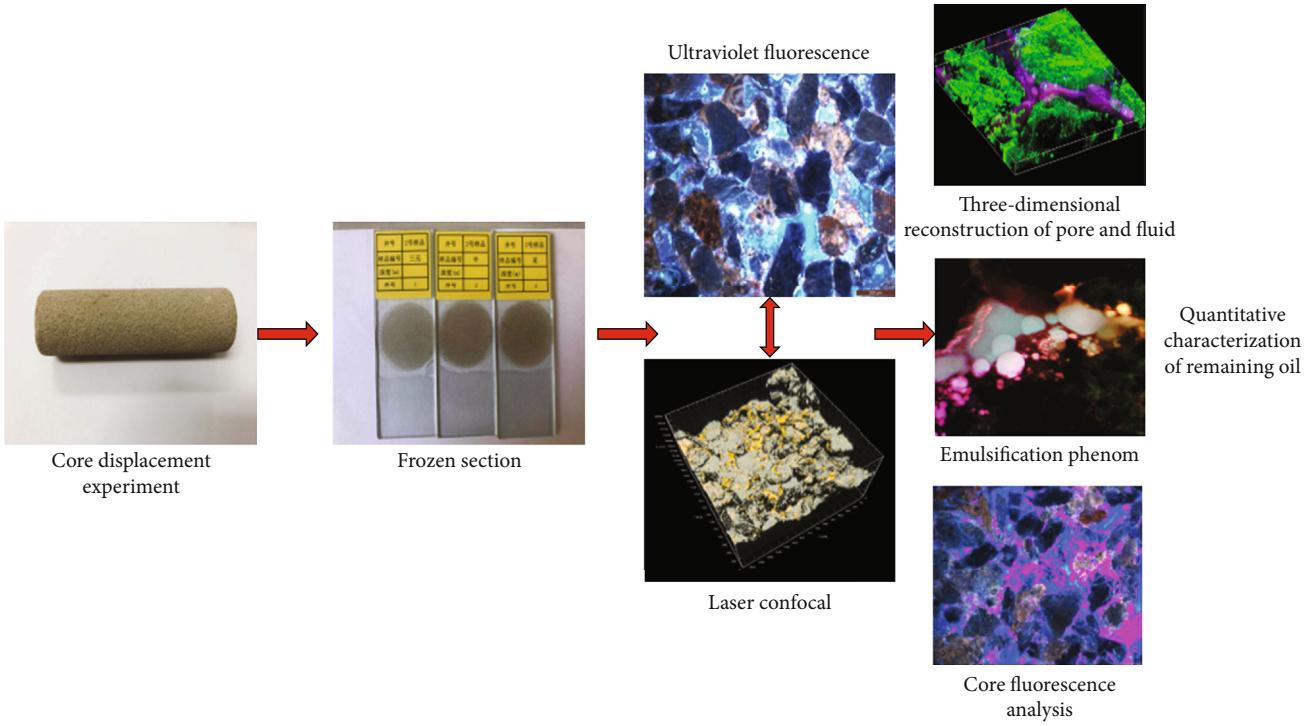

Figure 1: Quantitative analysis of remaining oil in frozen slicing.

Table 1: Component chemical parameters.

Type of medicine	Effective content (%)	Manufacturer
Polyacrylamide (molecular weight of 12 million)	90	Daqing refining and chemical company
Petroleum sulfonate	40	Daqing refining and chemical company
Sodium carbonate	99	Daqing refining and chemical company

Table 2: Core parameters.

Core type	Length (cm)	Diameter (cm)	Gas log permeability ($10^{-3}\mu m^2$)	Effective permeability ($10^{-3}\mu m^2$)	Porosity (%)
Natural sandstone core	10	2.5	2200	650	29.8

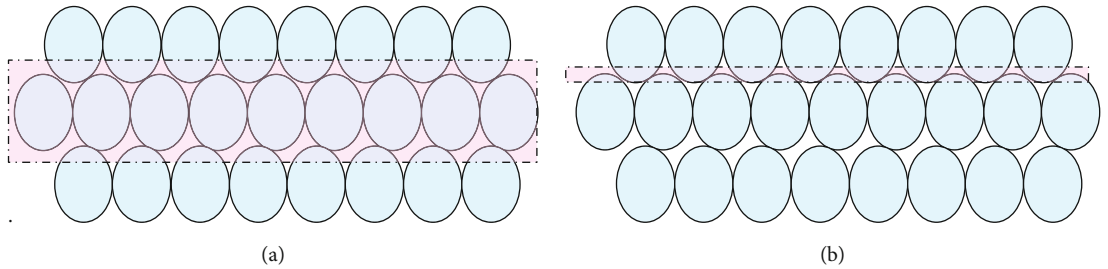

Figure 2: Difference between conventional and frozen production. (a) Conventional slicing method (room temperature production). (b) Frozen production method (liquid nitrogen frozen tablets).

generated during the cutting process, which can affect oil saturation, liquid nitrogen nozzles were installed at the cutting blade and core to cool them continuously. The hand-held oil-bearing sandstone grinding device was used for tablet production. The tableting process had to be conducted under low-temperature freezing conditions, which affects the test results. The finished product is shown in Figure 3(b).

The difference between laser confocal and ordinary optical microscopy is that ordinary optical microscopy uses a field light source, while confocal microscopy uses a laser

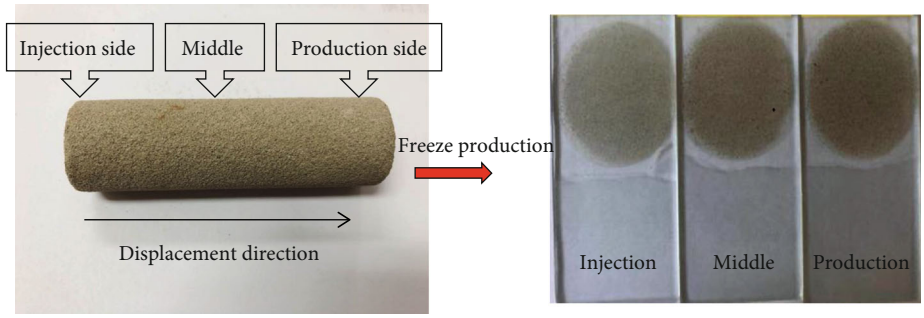

Figure 3: Core slice making process. (a) Natural core. (b) Freeze production after flooding experiment.

as the point light source. Because of the effect of light scattering, an ordinary microscope observes an interfering image, which affects the clarity and resolution of the image. However, the laser confocal scanning microscope image uses a point light source and a pinhole diaphragm to avoid the interference of light scattering. The positions of the incident light source pinhole and detection pinhole are conjugated with the focal plane of the objective lens [13–15]. Through the placement of a detection pinhole on the optical path of the emitted light, the light from the focal plane can be detected through the detection pinhole and the light from the focal plane. The light outside the plane is blocked on both sides of the pinhole, which is the basic principle of laser confocal microscopy, as shown in Figure 4(a). Confocal scanning in the plane direction involves scanning of the sample point-by-point or line-by-line to obtain a two-dimensional image. By means of scanning of the plane images of different axis positions at a certain interval in the longitudinal axis direction through three-dimensional reconstruction technology, the three-dimensional space state of the sample can be restored, as shown in Figure 4(b).

Crude oil contains a mixture of various fluorescent substances; different components have different fluorescence characteristics, and the intensity and color of fluorescence also differ. Therefore, the components of crude oil can be assessed on the basis of the color of the fluorescence [16–18]. Under the excitation of ultraviolet light, saturated hydrocarbons do not fluoresce, aromatic hydrocarbons generally appear blue-white, nonhydrocarbons usually appear yellow, orange, and brown, and asphaltenes appear red, brown, or even dark brown. Water does not emit light under a fluorescence microscope; however, the water in the pores dissolves traces of aromatic hydrocarbons and emits a lighter blue color. The fluorescent color can be used to distinguish oil and water. The relationship between the fluorescent color of crude oil and its components is summarized in Table 3.

The ordinary fluorescence microscope was excited by blue light, and the green filter was used to obtain the oil–water–rock image. The oil emits yellow-brown fluorescence, and the water emits yellow fluorescence [19]. In addition, the original slicing method involves a core slice thickness of 1 mm, which can easily cause the particles to be blocked upward and downward, thereby rendering it difficult to distinguish the pores and particles, as shown in Figure 5(a). The improved fluorescence microscope employs an ultraviolet excitation method; the full-band filter receives image information, and the oil–water–rock interface is clear (Figure 5(b)). The liquid nitrogen freezing film preparation technology ensures that the thickness of the core slice is the same when the crude oil composition is unchanged. The thickness can be up to 0.05 mm to avoid particle blocking and the residual oil occurrence state; the oil–water interface can be seen as a high-resolution clear image and provide quantitative parameters of the oil–water ratio to ensure the accuracy of the analysis results.

3. Results

3.1. Three-Dimensional Reconstruction of Laser Confocal Characterization of Oil–Water Distribution. Figure 6 shows a confocal laser scanning image of the different components of oil-bearing flake crude oil. Figure 6(a) shows the confocal laser scanning image of the oily thin slice. The green part G represents saturated hydrocarbons, which are liquid low-chain components adsorbed on the surface of mineral particles or pore walls; the corresponding scan curve is G1. The blue dotted part U represents the nonhydrocarbon organic matter component; the corresponding scan curve is U1. I represents a compound hydrocarbon component, which includes asphalt, aromatic hydrocarbons, and nonhydrocarbon organic matter, and F and L are the laser scanning curves of the aromatic hydrocarbons and asphaltenes, respectively. The blue dotted part U is separated from the compound hydrocarbons and exists in the free pores (black part) as a residue, which is washed with water. As a result of the combined effect of hydrodynamics, the abovementioned features can be seen more clearly from the three-dimensional reconstructed image of Figure 6(c). These results clearly reflect the oil displacement effect and characteristics. This method can retain the original state of the fluid inside the core to the greatest extent, and it causes the least damage to the core structure, thereby providing an effective and intuitive technical means for the comprehensive planning of subsequent development.

The three-dimensional observation and reconstruction analysis of oil, water, and rock indicates that most microcracks and micropores are connected. The results of the laser confocal experimental analysis indicates that the distribution characteristics of microscopic oil, water, and rock can be

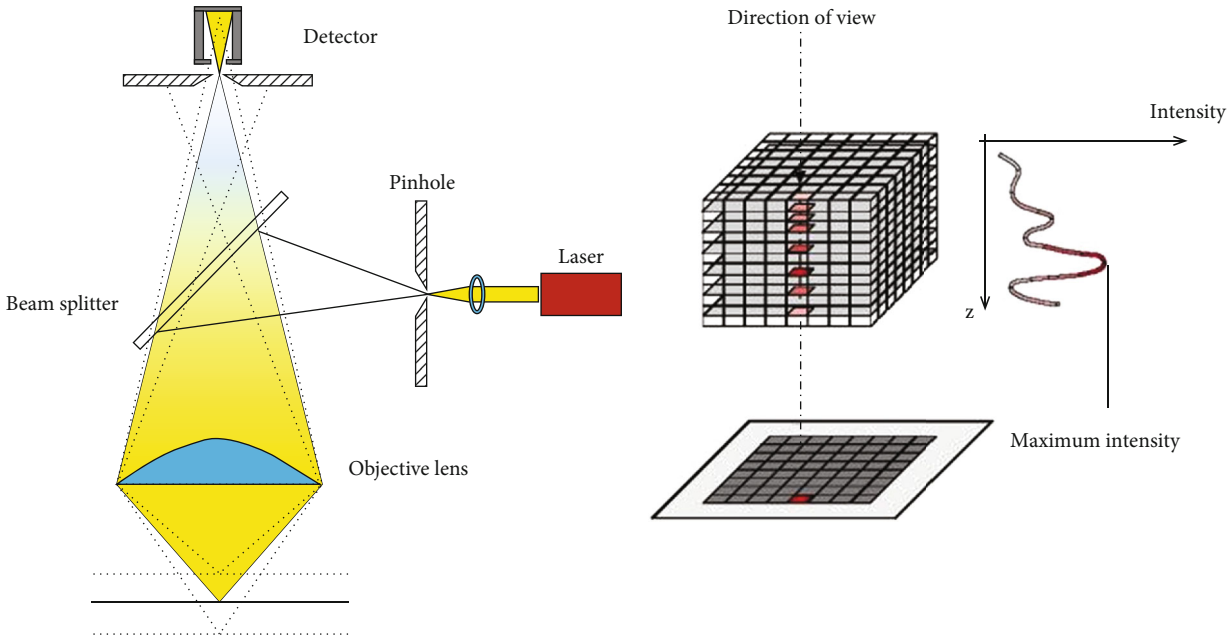

Figure 4: Principle and three-dimensional reconstruction of laser confocal scanning microscope. (a) Schematic. (b) XY plane scanning at different z-axis positions.

Table 3: Relationship between luminous color and crude oil composition.

Crude oil components	Glow color
Aromatics	Blue; blue and white; and light blue and white
Oily bitumen	Yellow, yellow-white, light yellow-white, green-yellow, light green-yellow, yellow-green, light yellow-green, green, light green, blue-green, light blue-green, green-blue, and light green-blue
Colloidal asphalt	Mainly orange, brown-orange, light brown-orange, light orange, yellow-orange, and light yellow-orange
Asphalt	Mainly brown, brown, light brown, orange-brown, light orange-brown, yellow-brown, and light yellow-brown
Carbonaceous pitch	No light (all black)

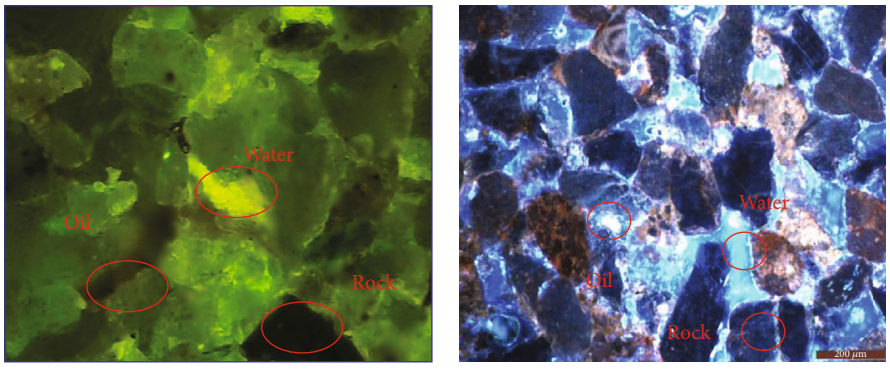

Figure 5: Distribution characteristics of oil, water, and rocks. (a) Blue light excitation. (b) UV excitation.

determined. Figure 7 shows a three-dimensional distribution map of microscopic light, heavy oil, and rock detected via laser confocal microscopy. As seen in Figure 7(b), light components are distributed in intergranular and intragranular pores. The distribution is primarily in the intergranular pores, and the intragranular distribution is low; further, the

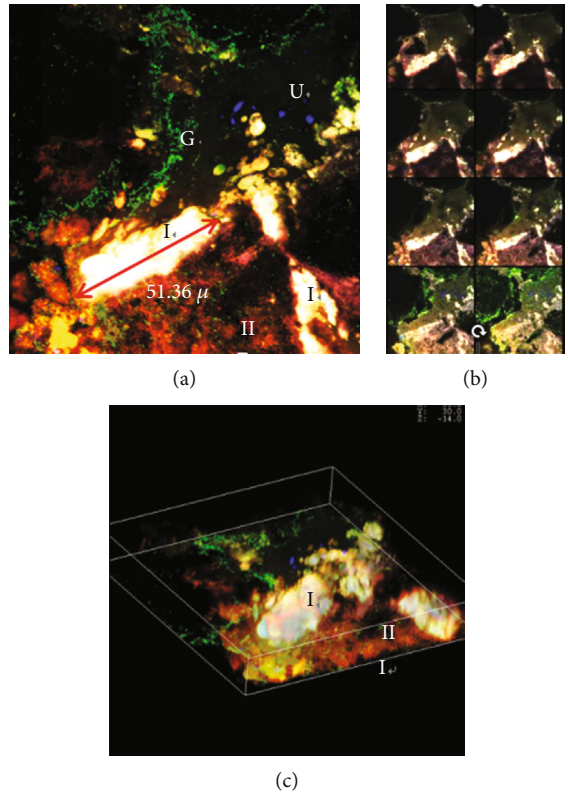

Figure 6: Laser confocal scanning image of different components of crude oil. (a) Laser confocal scanning image of oily sheet. (b) Series of images of the z-axis layered scanning in the same field of view. (c) 45° 3D reconstructed image of the same field of view.

light component of this sample is found to be 0.47 times lighter than the heavy component, according to the results of the confocal laser fluorescence detection analysis. The proportion of heavy oil has increased significantly, which indicates that many light oils have been driven out by water.

Figure 8 shows a microscopic three-dimensional distribution map of oil–water–rock. Figure 8(a) depicts a three-dimensional reconstruction image of the spatial distribution of oil and water, Figure 8(b) depicts that of rock pores, and Figure 8(c) depicts that of a fluorescent image of oil-containing slices. The three-dimensional observation and reconstruction analysis of oil, water, and rock indicates that most microcracks and pores are connected. During the preparation of core slices, multiple slices are obtained on each side by slicing at different positions of a single core. The different types of microscopic residual oil can be quantified accurately using domain analysis.

3.2. Microscopic Residual Oil Occurrence State. There exist various forms of microresidual oil in the formation. Depending on the occurrence and distribution characteristics of oil and water in the pores, microresidual oil can be categorized as follows: (1) bound-state residual oil adsorbed on the reservoir wall, which can be further categorized into pore-shaped film-like, particle-adsorbed, and slit-shaped residual oil; (2) semibounded residual oil at the edge of the bound state or away from the pore surface, which can be further categorized into corner-like and throat-like residual oil; and (3) the free oil remaining in the pores in the free state that is not in contact with the pores, which can be further categorized into cluster-like and intergranular adsorption oils [20].

3.2.1. Bound State. The film-like residual oil on the surface of pores is adsorbed on the surface of the rock mineral particles in the form of a thin film. The rock surface is oleophilic, and such a residual oil can exist on the surface. Therefore, the viscosity increase, peeling effect, and shear force of the polymer are observed. This type of residual oil has a certain effect; however, the effect is not obvious because the reservoir wettability cannot be changed, and displacing this type of residual oil completely is difficult (Figure 9(a)). Particulate adsorbed residual oil is distributed in uneven and high clay content. The reservoir particle surface, pore wall surface, and interstitial material exhibit strong adsorption capacities, which renders this part of the residual oil more difficult to displace (Figure 9(b)). The slit-shaped residual oil exists in the slender and narrow gaps less than 0.01 mm thick mainly in the dissolution pores or particle cracks of layered minerals, such as feldspar and mica, and as oil-bearing layered particles in kaolinite and chlorite particles. Such a residual oil exists in texture cracks [21], as shown in Figure 9(c).

3.2.2. Semibound State. The corner-shaped residual oil is stored in the "U"-shaped structure formed by the complex pore structure. An angle depression formed by one side contacts with different parts of reservoirs, and the other side contacts the open space in a free state. In the displacement process, this type of residual oil is partially displaced by the

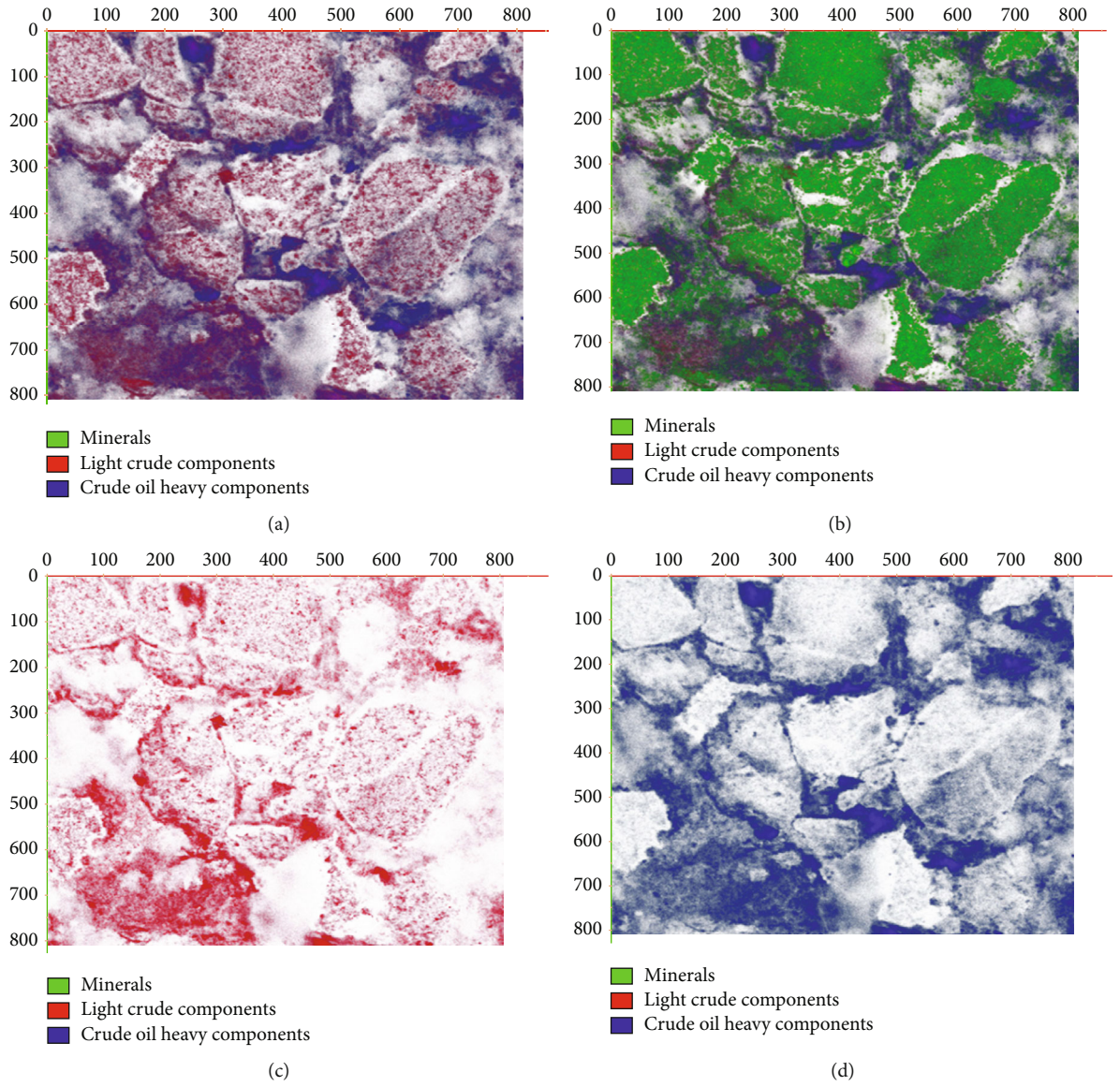

Figure 7: Microscopic light and heavy oil and rock distribution characteristics. (a) Overlay of distribution of light and heavy components in minerals and crude oil. (b) Overlay of distribution of light and heavy components in crude oil. (c) Distribution map of light components of crude oil. (d) Distribution map of heavy components of crude oil.

pulling and shear deformations of the polymer solution. To use this residual oil, it is necessary to increase the driving force and reduce the oil–water interfacial tension, as shown in Figure 10(a). The throat-like residual oil is stored in the small pore throat. Water flooding can displace the residual oil at the larger pore throat; however, oil is formed in the mosaic-like reservoir where the debris particles are in close contact with the capillary force. The slender curved throats contain a throat-like residual oil. Such a residual oil presents a continuous distribution in small pores, low-permeability reservoirs, or areas that are not affected by the displacement fluid (Figure 10(b)).

3.2.3. Free State. The cluster-like residual oil is stored in the pore space and distributed in clusters, oil beads, and clumps. After water flooding, this type of residual oil is distributed in an area that is not affected by the displacement agent, and it communicates with multiple pores. Owing to an insufficient driving force, water flooding has limited reach, and a large part of the oil remains in the formation, as shown in Figure 11(a). Intergranular adsorbed residual oil is distributed in regions with a high content of mud and clay. Although this type of residual oil is in a free state, it is mixed with clay debris and may migrate with the oil displacement system. Particles break, deform, and block the throat, resulting in a decrease in permeability, which causes the residual oil to remain in the pores (Figure 11(b)).

After the oil flooding experiment was completed, 2 cm thick slices were intercepted at the injection, middle, and production positions of the core to freeze and slice; the

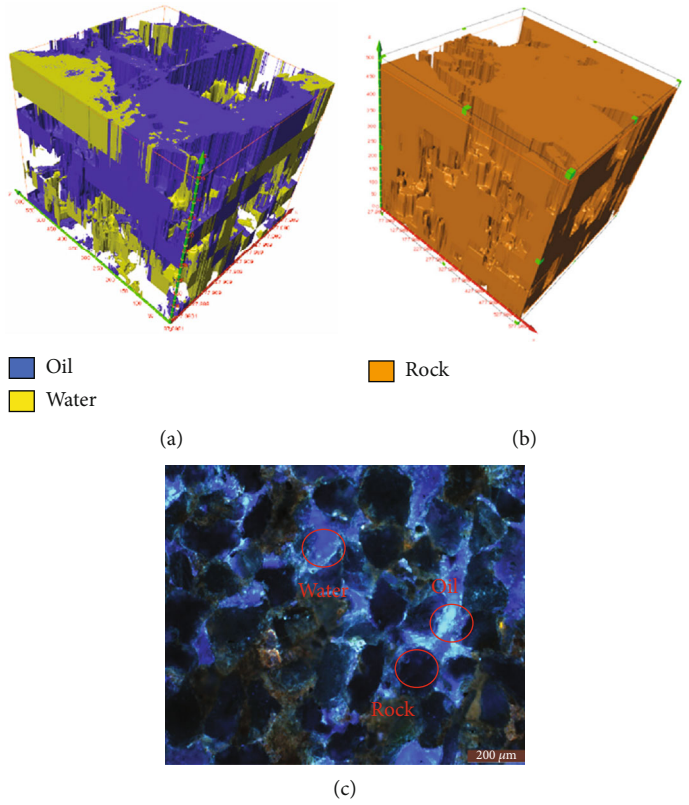

Figure 8: Three-dimensional distribution characteristics of microscopic oil–water rocks. (a) Three-dimensional reconstruction image of oil–water spatial distribution. (b) Three-dimensional reconstruction image of spatial distribution of rock pores. (c) Fluorescent images of oily flakes.

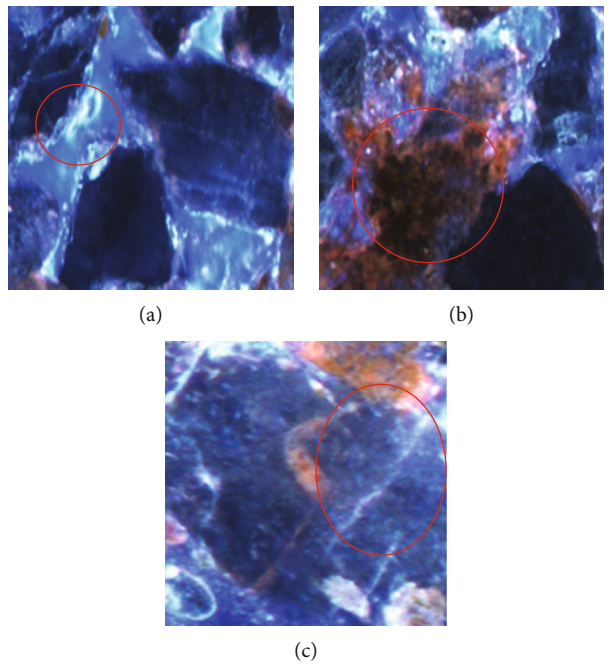

Figure 9: Residual oil in bound state. (a) Hole surface film. (b) Particle adsorption. (c) Slit-like.

microscopic residual oil after water flooding, polymer flooding, and ternary compound flooding was quantified using core fluorescence analysis software, as shown in Figure 12. The pink regions in the figure represent the residual oil; the amount of residual oil in the visual field was greater after water flooding. With the enhancement of the displacement

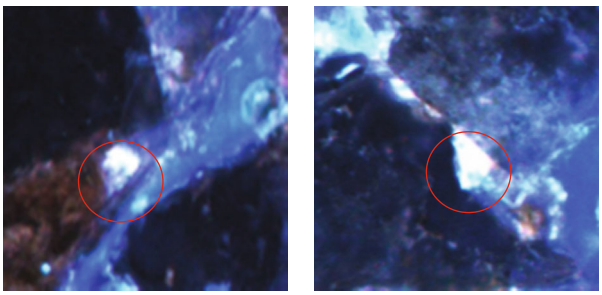

(a) (b)

Figure 10: Semibound residual oil. (a) Corner-shaped. (b) Throat-like.

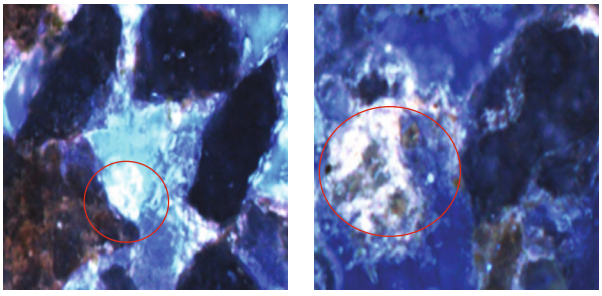

(a) (b)

Figure 11: Free-state residual oil. (a) Cluster. (b) Intergranular adsorption.

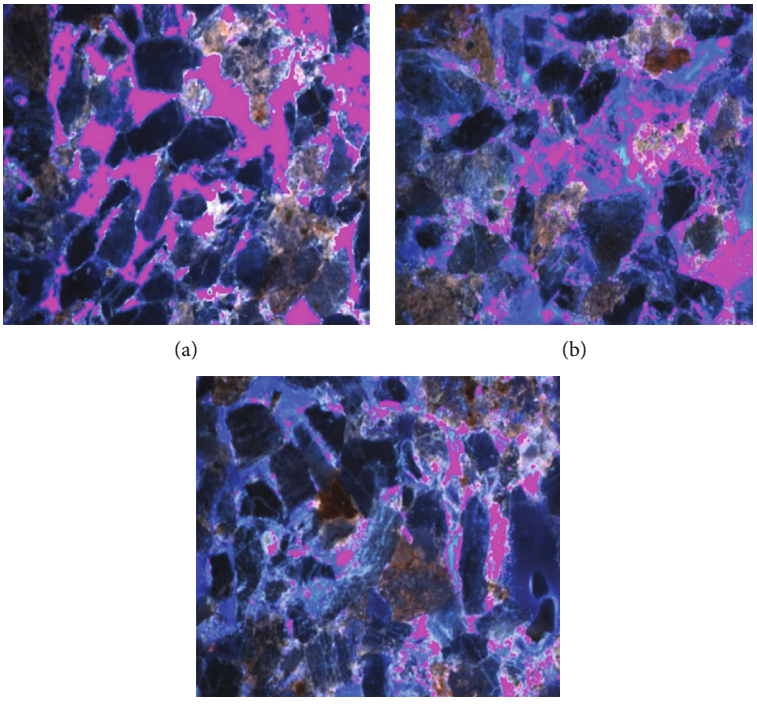

(a) (b)

(c)

Figure 12: Fluorescence analysis results after different displacement methods (the pink mark is residual oil). (a) Water flooding. (b) Polymer flooding. (c) ASP flooding.

Table 4: Absolute proportion of microscopic residual oil (each oil content in the table is the average of 20 analysis results).

Displacement method	Position	Different types of residual oil occurrence status and proportion (%)							Residual oil saturation in the field of view (%)	Residual oil saturation (%) in the core flooding experiment
		Bound state		Semibound state			Free state			
		Hole surface film	Particle adsorption	Slit-like	Corner-shaped	Larynx	Cluster	Intergranular adsorption		
Water flooding	Injection side	0.55	0.83	0.11	0.12	0.07	0.45	1.02	50.88	52.60
	Middle	0.95	0.92	0.31	0.30	0.09	0.91	1.65	51.32	
	Production side	2.53	1.76	0.32	0.38	0.12	1.10	2.48	53.98	
	Average	1.34	1.17	0.25	0.27	0.09	0.82	1.72	52.06	
Polymer flooding	Injection side	0.46	0.86	0.09	0.09	0.06	0.47	0.84	36.04	40.65
	Middle	0.50	0.91	0.24	0.13	0.07	0.64	1.05	38.44	
	Production side	1.70	0.98	0.25	0.24	0.10	0.77	2.04	42.09	
	Average	0.89	0.92	0.20	0.15	0.08	0.62	1.31	38.86	
ASP flooding	Injection side	0.37	0.72	0.08	0.07	0.04	0.35	0.71	27.25	30.93
	Middle	0.50	0.82	0.13	0.11	0.06	0.42	0.92	30.44	
	Production side	1.16	0.99	0.15	0.17	0.08	0.61	1.67	35.45	
	Average	0.68	0.84	0.12	0.12	0.06	0.46	1.10	31.05	

method, the remaining decline in the visual field after polymer flooding and after ternary compound flooding was greater.

On the basis of the abovementioned classification of microscopic residual oil, the quantitative analyses of different types of microscopic residual oil were conducted. To ensure that various types of residual oils did not overlap or leak during labeling and analysis, each type of residual oil was separately labeled, analyzed, and reported; an output was generated to confirm the accuracy of the analysis results. According to the results of Sun's laser confocal study [22], the actual oil content of the particulate adsorbed residual oil corresponds to one-tenth of the marked area.

The fluorescence analysis results of different flooding schemes were averaged statistics (Table 4). Under the same displacement mode, the proportion of residual oil at the injection, middle, and production ends increases sequentially because the sweep range is larger at the injection end. The increase in the seepage distance and the shearing, adsorption, and trapping effects of the formation on the solution reduces the control range of the oil displacement system and the oil displacement efficiency; therefore, there is an increase in the amount of residual oil. At the same position, the residual oil after water flooding is in the form of the bound pore surface film and particle-adsorbed oil and free-state cluster and intergranular adsorbed oil, with slit, corner, and throat residual oils. After ternary compound flooding, the residual oil type is particulate adsorbed, and the proportion of interparticle adsorption is larger. Because of the effect of the ternary system in terms of reducing the interfacial tension, the residual oil content in the pore surface film is significantly reduced, in contrast with the corners and throats. The proportion of the absolute area of the shape and slit shape in the entire visual field is small. Although the proportion is reduced, there is no obvious change in the other types of residual oil. From a morphological point of view, ternary compound flooding further reduces the free oil in the free state. A larger reduction is observed in the pore surface film in the bound state. The residual oil is adsorbed by the particles in the bound state and the interparticles in the free state. Adsorption is dominant, and the semibound state accounts for a small proportion. With the strengthening of the displacement means, an overall ratio change is still not obvious; this implies that the effect of the ternary compound flooding on this type of residual oil is also not obvious. The difference between residual oil saturation in the domain and that in the core flooding experiment is small, which verifies the accuracy of the fluorescence analysis results.

In consideration of the microscopic residual oil after water flooding as a whole (Table 4), the utilization degree of each type of residual oil after different flooding methods was calculated as shown in Figure 13. The residual oil after water flooding is in the free and bound states. The proportion of residual oil in the bound state is 48.78%, and that in the free state is 44.87%; further, that in the semibound state is only 6.35%. Because of the low viscosity of water and the insufficient driving force, the capillary force of multiple channels has a limited effect on cluster-like and intergranular adsorptive residual oil mixed with clay debris. Owing to the limited ability of polymer to reduce the interfacial tension, the oil is adsorbed in the pores. The residual oil in the form of a thin film, and granular adsorbed oil content on the pore

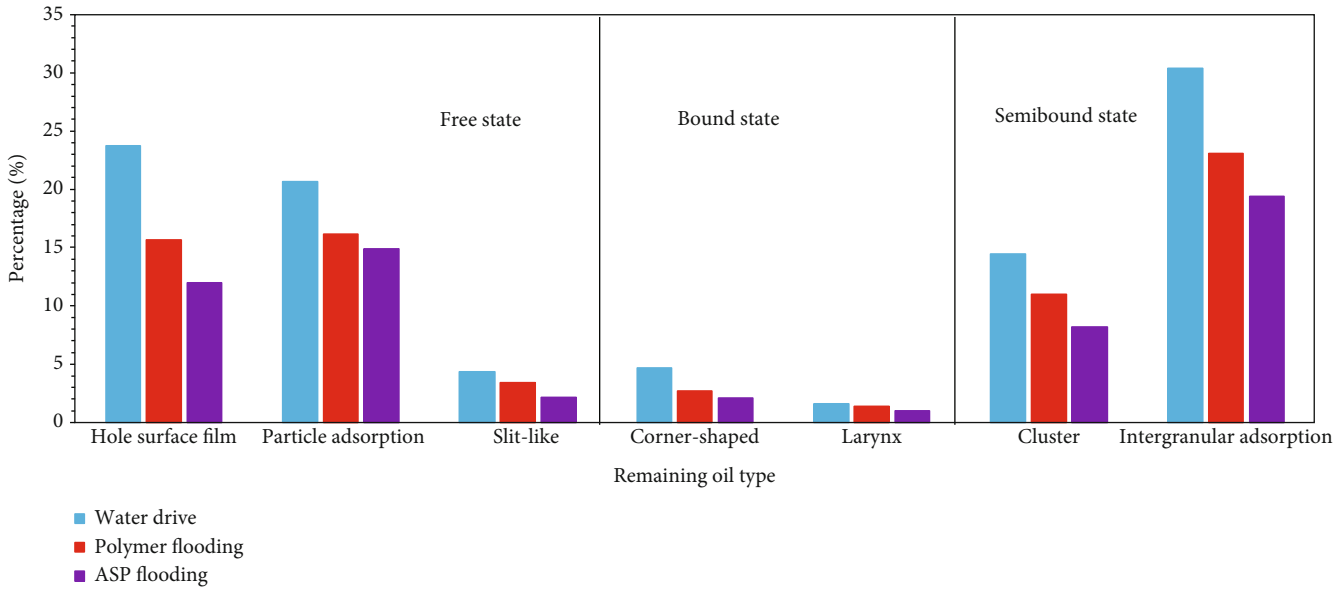

Figure 13: Microscopic residual oil producing degree after different displacement methods.

surface of the wall is also higher after water flooding; these contents correspond to 23.75% and 20.69%, respectively. Polymer flooding was carried out after water flooding. Given the increase in the viscosity of the flooding phase and the sweeping range, the effect on clusters and particles in the free state is obvious. The reduction ratios of the two are 23.85% and 23.87%, respectively. Because of the viscoelasticity of the polymer, the reduction ratio of the corner-shaped residual oil in the semibound state reaches 42.68%. Further, the viscosity-increasing, stripping, and shearing forces of the polymer have a certain effect on the bound residual oil. The bound residual oil is reduced by 13.48%; however, the effect is not obvious because the reservoir wettability cannot be changed, and the oil–water interfacial tension cannot be reduced. Moreover, it is difficult to displace such residual oil completely. Because of water flooding, the degree of polymer driving increases by 26.44%. Ternary compound flooding was performed after water flooding. Although the viscosity of the system is the same as that after polymer flooding, the interfacial tension reaches an ultralow order of 0.003 mN/m. While the remaining level of free oil increases, the oil–water interfacial tension reduces the surface energy adsorbed on the rock surface, thereby changing wall wettability, stripping the residual oil from the pore surface, and improving the utilization of the bound-state residual oil. After ternary composite flooding, the pore surface is film-like, particle-adsorbed, slit-shaped, corner-shaped, throat-shaped, and cluster-shaped; the intergranular adsorbed residual oil ratios correspond to 11.98%, 14.91%, 2.14%, 2.08%, 1.02%, 8.19%, and 19.45%, respectively. Owing to water flooding, the degree of utilization increases by 40.21%, 13.77% higher than that of polymer flooding. The highest proportion of residual oil after ternary compound flooding is of intergranular adsorbed, pore surface film, and particle adsorbed, which are the targets for potential tapping in the next step.

3.3. Analysis of Emulsification Characteristics in Porous Media. During chemical flooding, the concentration of the formed aqueous solution formed is greater than the critical micelle concentration because of the addition of alkali and surfactants. The micellar solution, which has ultralow interfacial tension, can solubilize oil and water to form swollen micelles, which is a microemulsion. After the microemulsion is formed during the displacement process, the fluidity of the crude oil is enhanced, which in turn enhances the emulsification carrying effect, thereby improving oil recovery. The Winsor phase diagram method is a common method used to study the behavior of the emulsion liquid. The microemulsion is composed of multiple components. During the displacement process, when the content of each component changes, the phase state of the microemulsion system changes [23]. When the concentrations of the surfactant and cosurfactant are fixed, and inorganic salt is added to the system, the system balances the two phases of the lower-phase microemulsion (O/W) and the residual oil phase. Figure 14(a) shows that after the middle-phase microemulsion, the residual oil phase and the water phase are in three-phase equilibrium. Figure 14(b) shows that this system is transformed into that of two-phase equilibrium of the upper-phase microemulsion (W/O) and the remaining water phase (Figure 14(c)).

A certain amount of ionic liquid (ternary composite system) was weighed in a test tube with a stopper, and water was added to dissolve it to a certain concentration. Then, the oil of equal quality (oil – water mass ratio rW/O = 1) was weighed, and n-butanol was added to the above test tube. Next, all samples were placed in a $40 \pm 0.1^{\circ}C$ water bath environment for approximately a week, the changes of each phase in the test tube were observed, and the volume of each phase when the volume no longer changed was recorded. Then, the contents of different ionic liquids were changed, and the above operation was repeated; finally, the Winsor

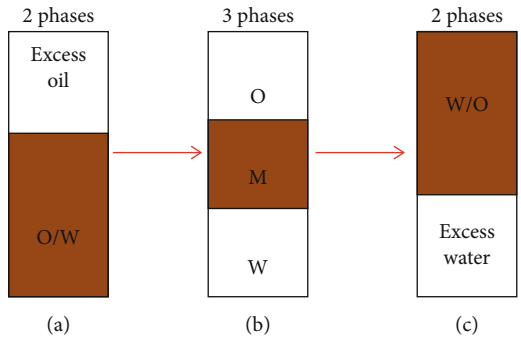

Figure 14: Winsor microemulsion type. (a) Winsor I. (b) Winsor II. (c) Winsor III.

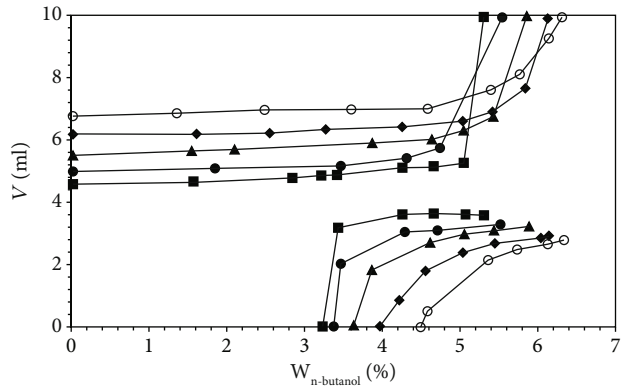

Figure 15: Influence of content of surfactant on the Winsor phase diagram.

phase diagram was created [24, 25]. As shown in Figure 15, as the amount of surfactant increases, the content of alcohol and the solubilizing ability of the system required to form the middle-phase microemulsion increases. As the content of surfactant increases, more alcohol molecules are needed to balance the interface layer; therefore, the alcohol width increases to change the size and direction of the interface curvature. As the content of surfactant increases, the alcohol width decreases. This can be explained by the fact that when the surfactant content is high, a large number of O/W droplets are present in the system, and they interact with each other, thereby promoting a change in the curvature of the interface layer. The curvature of the interface layer changes only slightly from the formation to the disappearance of the intermediate phase. The disappearance of the phase only changes slightly, which in turn leads to a decrease in the alcohol width. The alcohol content and the mass ratio of the surfactant and the alcohol width indicate that the decrease in the mass ratio of the active agent is caused by the distribution of alcohol in the oil phase. A part of the alcohol is distributed in the interface layer, and another part is distributed in the oil phase of the microemulsion. With an increase in the surfactant content, the distribution of alcohol in the oil phase decreases, which leads to a decrease in alcohol content and alcohol width.

The pressure change during the oil displacement process in the ternary composite system can reflect the change in the emulsion liquid state, as shown in Figure 16. During water flooding and the subsequent water flooding processes, the pressure difference of each section along the flow direction fluctuates very little. The solution form exists in the form of Winsor I if the pressure difference is caused by the low surfactant content in this process. In the process of ternary composite system flooding, the highest pressure difference attained in each section along the flow direction gradually increases. When the injected liquid moves to 2/3 of the core, the pressure difference in this section rises to twice that of the inlet section, attains the maximum value, and then decreases. This is because the surfactant concentration increases as the volume of the injected solution increases, which increases the emulsification carrying capacity of the displacement fluid. The high-viscosity emulsion produced during the displacement process changes the phase state of the solution from Winsor III to Winsor II. During the displacement process, the emulsion preferentially enters the high-permeability layer and produces a certain blocking effect on these layers; therefore, the medium- and low-permeability horizon activation expands the sweep efficiency of ASP flooding. The emulsification phenomenon is manifested by an increase in the displacement pressure difference. The most important contribution of emulsification to oil displacement is emulsification carrying and emulsion profile control. Emulsification carrying is a ternary composite system with ultralow interfacial tension. Through reduction in the interfacial tension, the capillary, cohesive, and viscous forces are greatly reduced, which causes the erosion of the oil formed without type emulsion to flow easily. This stage exists in the form of Winsor II, after which an oil wall is formed through coalescence, thereby enhancing oil recovery.

The formation of emulsions in the process of oil displacement plays a considerable role in improving oil recovery; therefore, emulsification performance is an important indicator for evaluating the pros and cons of the composite system. The high-density O/W emulsion droplets generate a good carrying effect on the residual oil in the formation, thereby effectively starting the crude oil, emulsifying the started crude oil, and carrying it to the production well. The carrying effect is affected by the permeability, gravity, mass concentration of the dispersed phase in the emulsion, respective density of the two phases, and interfacial tension. If a W/O emulsion is formed, it is understood that an oil wall is formed; the oil wall generates a strong carrying effect on the residual oil/residual oil, which can greatly improve the oil displacement efficiency. The microscopic images of the emulsion produced at the wellhead of the ASP flooding represent the complex transformation process of the emulsion—that is, how heavy the emulsion may appear during the transition from O/W to W/O. The emulsion is of the Winsor I (O/W) type at the beginning of the displacement. As the displacement progresses, a Winsor III (O/M/W) type emulsion appears, in which medium-phase microemulsion, oil, and water coexist. The increase in surfactant concentration has a significant effect on reducing the oil–water interfacial tension and is also beneficial to the stability of the emulsion. Therefore, interfacial tension and emulsification are complementary properties that do not conflict with one another. Low interfacial tension can promote emulsification.

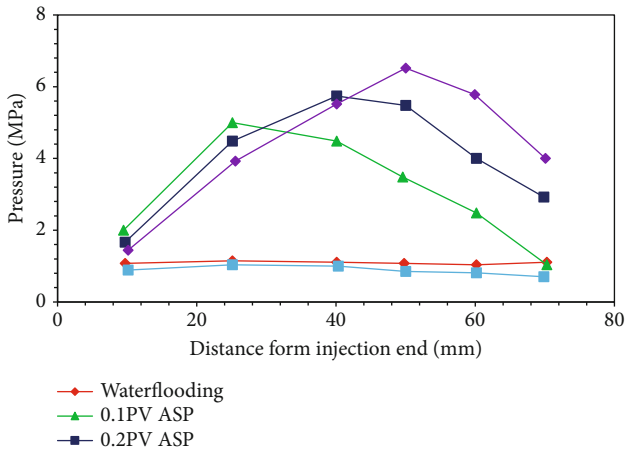

Figure 16: Pressure variation curve of ASP flooding process.

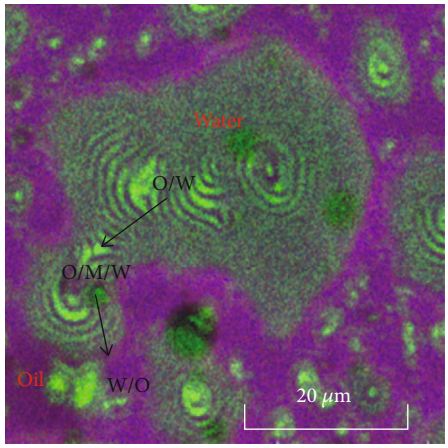

Figure 17: Emulsion transformation process.

Therefore, after a period of displacement by the ternary composite system flooding, the emulsion type is finally changed to Winsor II (W/O), as shown in Figure 17.

3.4. Cause Analysis of Residual Oil

3.4.1. Pore Structure. Owing to the microheterogeneity of the pore medium, precipitation clusters of uneven sizes are formed at the center of the pore; this causes the displacement phase to advance along the channel with low resistance during displacement because of the injection speed, displacement pressure, and factors such as the pore structure that causes an insufficient driving force to give rise to a fingering phenomenon (Figure 18). Once the dominant channel is formed, a trapping effect is generated on a part of the pores or residual oil, and a flow phenomenon occurs, leading to formation of a cluster of microscopic residual oil [26]. A cluster-like residual oil is formed because of complex flow field changes. The more complicated is the distribution of pore throats, the greater is the pore-throat ratio, and the greater is the proportion of formed cluster-like residual oil.

3.4.2. Crude Oil Viscosity. Crude oil emulsifies to varying degrees as it moves through the pores. In hydrophilic media, the bound water exists in the form of water beads, and the oil fills the entire pore system. During the displacement process, the viscosity resistance of the crude oil and the pore surface must be overcome. Meanwhile, the viscosity of water is lower than that of oil. Channeling in the center of the pores leaves a thin oil film of varying thickness on the pore surface (Figure 19). As the displacement strength increases, the oil-in-water residual oil is produced. In the oleophilic medium, the nonwetting phase displaces the wetting phase [27]. Water advances along the central axis of the pores, and it cannot easily advance along the pores in the vertical flow direction. The water-in-oil residual oil is formed after polymer flooding. The viscosity of crude oil increases, and the resistance to migration also increases, resulting in cluster-like residual oil formation.

3.4.3. Jia Min Effect. In reservoirs with poor pore connectivity, pore throats that lead to the blockage of residual oil and blockage are prone to form owing to particle migration and changes in interfacial tension. The blocking of multiple pore throats causes a large amount of oil to be trapped in the concealed corners, wherein one side is attached to the contact of the particles, and the cutoff corresponds to the original continuous oil beads or columnar residual oil separated into small isolated oil droplets [28]. When these bubbles or oil droplets pass through the small pore throat because of the pores, the difference in the radius of the throat causes the capillary forces on the ends of the bubbles or oil droplets to act as a resistance (Figure 20). To pass through the throat with a smaller radius, the droplet must elongate and change its shape. This deformation consumes energy and slows down the bubbles or oil droplets; further, movement adds additional resistance. Because the pores in which the oil beads are located are larger, and the pore throats connected to them are smaller, the oil beads are difficult to drive away owing to the Jia Min effect; thus, they form corner-like residual oil.

3.4.4. Particle Migration. When residual oil exists in open pores but still adheres to the surface of clay minerals when the displacement phase is injected into the formation, particle deformation, fragmentation, and migration are caused [29]. This phenomenon usually occurs in reservoirs with high or medium high permeability, clay and rock debris migrate, particles and crude oil are locally enriched, throats are blocked, reservoir permeability reduces, viscosity changes, and fluidity deteriorates, which affects residual oil recovery; this leads to the production of intergranular adsorbed residual oil. The mixture can be removed with the flow of fluid in the reservoir. As the displacement strength increases, the intergranular filler decreases, and such residual oil content also decreases (Figure 21).

3.4.5. Particle Surface Adsorption. The surface of the rock particles is positively or negatively charged; further, the asphaltene in the crude oil component is charged (Figure 22). According to the adsorption force on the surface of the

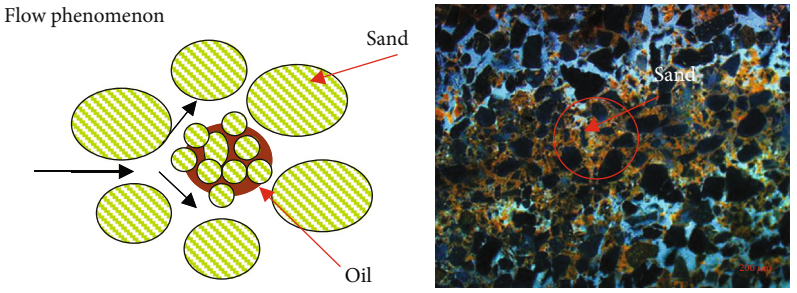

Figure 18: Reasons for residual oil formation caused by changes in pore structure. (a) Schematic. (b) Fluorescent picture.

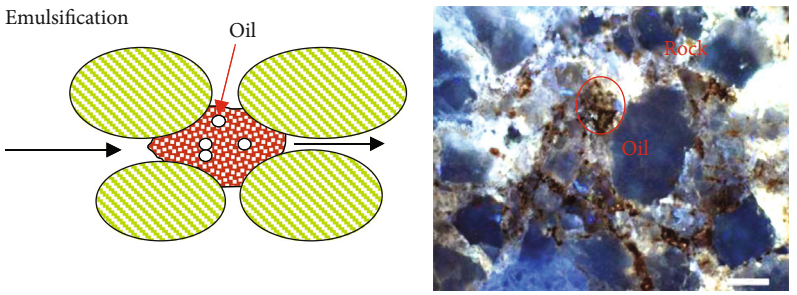

Figure 19: Reasons for changes in crude oil viscosity to form residual oil. (a) Schematic. (b) Fluorescent picture.

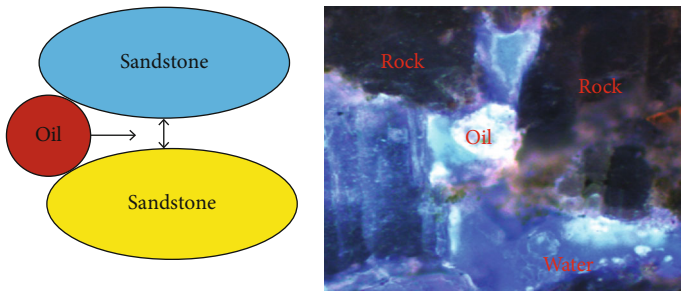

Figure 20: Reasons for formation of residual oil via Jia Min effect. (a) Schematic. (b) Fluorescent picture.

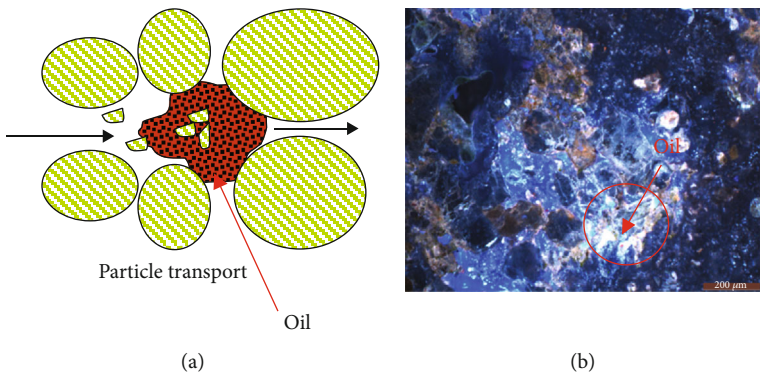

Figure 21: Causes for residual oil generation via particle migration. (a) Schematic. (b) Fluorescent picture.

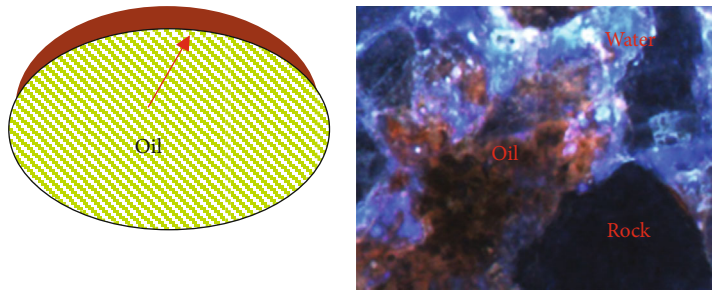

(a) (b)

Figure 22: Reasons for residual oil production via adsorption force on the surface. (a) Schematic. (b) Fluorescent picture.

particles, film-like residual oil and throat-like residual oil on the pore surface are generated [30], and the capillary force produces a slit-like residual; oil and particles adsorb the residual oil.

4. Discussion

This study employed a combination of laser confocal, cryopreservation technology, and core fluorescence analysis technology to perform the three-dimensional reconstruction of oil, water, and rock in the core. The components of crude oil could be analyzed, oil and water could be quantitatively characterized, and emulsification characteristics in the porous medium could be observed more clearly. The research results obtained using this method clearly reflect the oil displacement effect and characteristics. This method can retain the original distribution state of the fluid inside the core to the greatest extent, cause the least damage to the core structure, and provide an effective and intuitive technical means for the comprehensive planning of subsequent development.

5. Summary and Conclusions

The conclusions of this study are listed as follows.

(1) A confocal laser was used to reconstruct the distribution characteristics of oil, water, and rock in oil-bearing thin slices. According to the different reflection colors of different components in the crude oil, the microscopic residual oil and porous media after ASP flooding were described, and the type of emulsion was distinguished

(2) The cores processed under different flooding methods were frozen and sliced, and different positions and different types of residual oil were quantitatively characterized. The residual oil saturation at the injection, middle, and production ends increased sequentially. After ASP flooding, the particle adsorption state and the adsorption state between the particles showed the highest residual oil saturation; this provides the cue to tap the potential thereof

(3) With 60 fields of view considered in each core for the analysis, the difference between the residual oil saturation in the fluorescence analysis of different displacement methods and the residual oil saturation of the core flooding experiment was found to be very small, which verified the correctness of the fluorescence analysis data

(4) The influence of the surfactant ion concentration on the Winsor phase diagram was analyzed, and the microscopic image was used to characterize the transformation process of the microemulsion from Winsor I→Winsor III→Winsor II

(5) Through fluorescence images, the reasons for the formation of different types of microscopic residual oil were analyzed. These reasons include pore structure, crude oil viscosity, the Jia Min effect, particle migration, and particle surface adsorption.

Data Availability

The data used to support the findings of this study are available from the corresponding author upon request.

Conflicts of Interest

We would like to submit the enclosed manuscript titled "Microscopic residual oil distribution characteristics and quantitative characterization of producing degree based on core fluorescence analysis technology," for publication in *Geofluids*. No conflict of interest exists regarding the submission of this manuscript, and the manuscript has been approved by all authors for publication. I would like to declare on behalf of my coauthors that the research described was original, has not been published previously, and is not under consideration for publication elsewhere, in whole or in part. All the authors listed have approved the enclosed manuscript.

Acknowledgments

This research was conducted at the Key Laboratory of Enhanced Oil & Gas Recovery of the Ministry of Education at Northeast Petroleum University (Daqing, China). The authors gratefully acknowledge the support of the National Natural Science Foundation of China (No. 51574089) and Heilongjiang Provincial Department of Education (TSTAU-R2018018), and the Innovative Scientific Research Project for Postgraduates of Northeast Petroleum University (YJCX2016-013NEPU).

References

[1] M. Kamyab, M. Dejam, M. Masihi, and M. H. Ghazanfari, "The gas-oil gravity drainage model in a single matrix block: a new relationship between relative permeability and capillary pressure functions," *Journal of Porous Media*, vol. 14, no. 8, pp. 709–720, 2011.

[2] M. Dejam, M. H. Ghazanfari, V. Mashayekhizadeh, and M. Kamyab, "Factors affecting the gravity drainage mechanism from a single matrix block in naturally fractured reservoirs," *Special Topics & Reviews in Porous Media - An International Journal*, vol. 2, no. 2, pp. 115–124, 2011.

[3] J. Dakhelpour-Ghoveifel, M. Shegeftfard, and M. Dejam, "Capillary-based method for rock typing in transition zone of carbonate reservoirs," *Journal of Petroleum Exploration and Production Technology*, vol. 9, no. 3, pp. 2009–2018, 2019.

[4] H. Saboorian-Jooybari, M. Dejam, Z. Chen, and P. Pourafshary, "Comprehensive evaluation of fracture parameters by dual Laterolog data," *Journal of Applied Geophysics*, vol. 131, pp. 214–221, 2016.

[5] A. Sugar, M. F. Serag, V. A. Torrealba, U. Buttner, S. Habuchi, and H. Hoteit, "Visualization of polymer retention mechanisms in porous media using microfluidics," in *SPE Europec featured at 82nd EAGE Conference and Exhibition*, Amsterdam, The Netherlands, 2020, June 8.

[6] M. K. Verma, M. Boucherit, and L. Bouvier, "Evaluation of residual oil saturation after waterflood in a carbonate reservoir," *SPE Reservoir Engineering*, vol. 9, no. 4, pp. 247–253, 1994.

[7] X. SUN, W. TANG, and X. YU, "The key technology of micro area visualization in the application of the oil and gas exploration and development," *Acta Geologica Sinica - English Edition*, vol. 89, no. s1, pp. 405–408, 2015.

[8] D. I. Qinfeng, J. ZHANG, S. HUA, H. CHEN, and C. GU, "Visualization experiments on polymer-weak gel profile control and displacement by NMR technique," *Petroleum Exploration and Development*, vol. 44, no. 2, pp. 294–298, 2017.

[9] C. W. J. Sorber, G. A. M. Ketelaars, E. S. Gelsema, J. F. Jongkind, and W. C. Bruijn, "Quantitative analysis of electron energy-loss spectra from ultrathin-sectioned biological material," *Journal of Microscopy*, vol. 162, no. 1, pp. 23–42, 1991.

[10] J. T. Edwards, M. M. Honarpour, R. D. Hazlett et al., "Validation of gravity-dominated relative permeability and residual oil saturation in a giant oil reservoir," in *SPE Annual Technical Conference and Exhibition*, New Orleans, Louisiana, 1998.

[11] Y. Li, Y. Yang, X. Sun et al., "The application of laser confocal method in microscopic oil analysis," *Journal of Petroleum Science and Engineering*, vol. 120, pp. 52–60, 2014.

[12] X. Gu, C. Pu, N. Khan, F. Wu, F. Huang, and H. Xu, "The visual and quantitative study of remaining oil microoccurrence caused by spontaneous imbibition in extra-low permeability sandstone using computed tomography," *Fuel*, vol. 237, pp. 152–162, 2019.

[13] H. X. Sun, Y. J. Zhao, and J. Yao, "Micro-distribution and mechanical characteristics analysis of remaining oil," *Petroleum*, vol. 3, no. 4, pp. 483–488, 2017.

[14] T. Umakoshi, S. Fukuda, R. Iino, T. Uchihashi, and T. Ando, "High-speed near-field fluorescence microscopy combined with high-speed atomic force microscopy for biological studies," *Biochimica et Biophysica Acta (BBA) - General Subjects*, vol. 1864, no. 2, article 129325, 2020.

[15] Y. Li, J. Li, S. Ding, and X. Sun, "Characterization of residual oil after polymer flooding by laser scanning confocal fluorescence microscopy," *Journal of Dispersion Science and Technology*, vol. 35, no. 7, pp. 898–906, 2014.

[16] M. Yue, W. Zhu, H. Han, H. Song, Y. Long, and Y. Lou, "Experimental research on remaining oil distribution and recovery performances after nano-micron polymer particles injection by direct visualization," *Fuel*, vol. 212, pp. 506–514, 2018.

[17] K. Liu, P. Eadington, and D. Coghlan, "Fluorescence evidence of polar hydrocarbon interaction on mineral surfaces and implications to alteration of reservoir wettability," *Journal of Petroleum Science and Engineering*, vol. 39, no. 3-4, pp. 275–285, 2003.

[18] R. Decou, H. Serk, D. Ménard, and E. Pesquet, "Analysis of lignin composition and distribution using fluorescence laser confocal microspectroscopy," in *Methods in Molecular Biology*, Humana Press, New York, NY, 2017.

[19] D. F. Rucker, "Resistivity tomography with a vertical line current source and its applications to the evaluation of residual oil saturation," *Journal of Applied Geophysics*, vol. 86, pp. 160-161, 2012.

[20] P. F. Xiao, X. Y. Leng, H. M. Xiao et al., "Investigation effect of wettability and heterogeneity in water flooding and on microscopic residual oil distribution in tight sandstone cores with NMR technique," *Open Physics*, vol. 15, no. 1, pp. 544–550, 2017.

[21] P. P. Hu, F. L. Yang, W. Wang et al., "Thermal anomaly profiles inferred from fluid inclusions near extensional and strike-slip faults of the Liaodong Bay Subbasin, Bohai Bay Basin, China: implications for fluid flow and the petroleum system," *Marine and Petroleum Geology*, vol. 93, pp. 520–538, 2018.

[22] A. Mauko, T. Muck, B. Mirtič, A. Mladenovič, and M. Kreft, "Use of confocal laser scanning microscopy (CLSM) for the characterization of porosity in marble," *Materials Characterization*, vol. 60, no. 7, pp. 603–609, 2009.

[23] M. Wagner, N. P. Ivleva, C. Haisch, R. Niessner, and H. Horn, "Combined use of confocal laser scanning microscopy (CLSM) and Raman microscopy (RM): investigations on EPS – Matrix," *Water Research*, vol. 43, no. 1, pp. 63–76, 2009.

[24] S. Pfeiffer, M. Beese, M. Boettcher, K. Kawaschinski, and K. Krupinska, "Combined use of confocal laser scanning microscopy and transmission electron microscopy for visualisation of identical cells processed by cryotechniques," *Protoplasma*, vol. 222, no. 3-4, pp. 129–137, 2003.

[25] H. K. Nie and J. C. Zhang, "Control effect of fluid entry pressure on hydrocarbon accumulation," *Journal of Central South University of Technology*, vol. 17, no. 6, pp. 1395–1402, 2010.

[26] W. F. Pu, P. Wei, L. Sun, F. Y. Jin, and S. Wang, "Experimental investigation of viscoelastic polymers for stabilizing foam," *Journal of Industrial and Engineering Chemistry*, vol. 47, pp. 360–367, 2017.

[27] F. Feng, H. L. Zhang, Z. Q. Zhu, C. Li, Y. X. Shi, and Z. Y. Zhang, "The application of anti-ESAT-6 monoclonal antibody fluorescent probe in ex vivo near-infrared fluorescence imaging in mice with pulmonary tuberculosis," *Luminescence*, vol. 29, no. 6, pp. 614–620, 2014.

[28] W. C. Fang, H. Jiang, J. Li et al., "A new experimental methodology to investigate formation damage in clay-bearing reservoirs," *Journal of Petroleum Science and Engineering*, vol. 143, pp. 226–234, 2016.

[29] A. Victor, M. E. Rinaldi, and J. J. C. Zeballos, "Influence of shearing rate on residual strength of clays," *Advances in Soil Mechanics and Geotechnical Engineering*, vol. 58, no. 2, 2015.

[30] A. Xu, "Study on the relationship between internal heterogeneity of single sand body and remaining oil distribution in Pubei Oil Field," *IOP Conference Series: Earth and Environmental Science*, vol. 558, article 022035, no. 2, 2020.